JAAS

Particle generated spectral interferences in single particle ICP-MS: A roadblock to accurate nanometrology

Journal:	*Journal of Analytical Atomic Spectrometry*
Manuscript ID	JA-TEC-09-2023-000332.R1
Article Type:	Technical Note
Date Submitted by the Author:	28-Nov-2023
Complete List of Authors:	Goodman, Aaron; Colorado School of Mines, Chemistry Kanapilly, Sandra; PerkinElmer Inc Bednar, Anthony; U.S. Army Engineer Research and Development Center, Ranville, James; Colorado School of Mines, Chemistry

Particle generated spectral interferences in single particle ICP-MS: A roadblock to accurate nanometrology

Aaron J Goodman[1]*, Sandra Kanapilly[2], Anthony J Bednar[3], James F Ranville[1]

1. Department of Chemistry, Colorado School of Mines, United States of America
2. PerkinElmer, 940 Winter St. Waltham MA, United States of America
3. US Army Corps of Engineers, Engineer Research and Development Center, United States of America

*Corresponding Author

Abstract:

The recent expansion of single particle inductively coupled plasma mass spectrometry (spICP-MS) for analysis of inorganic nanoparticles (NPs) in environmental and laboratory samples requires continued method development to ensure accurate characterization. Spectral interferences in spICP-MS analysis are often not fully addressed, especially particle generated interferences. Discrete ion clouds from ablated NPs entering the plasma form doubly charged and polyatomic species in a manner similar to dissolved ions that contribute to the continuous background signal. spICP-MS analysis of Y- and Nd-NP suspensions resulted in NP detections that are falsely identified as Pd, Ge, and As NPs due to interferences of YO^+ and Nd^{2+}. Use of a dynamic reaction cell (DRC) eliminated YO^+ interferences, while Pd NPs were still accurately measured in mixed suspensions of Pd- and Y-NPs. A strong correlation was observed between the magnitude of interferences in solution mode and single particle mode, supporting a similar mechanism of interferent formation in the plasma for dissolved and NP-associated ions. Additionally, interference formation was affected by changes in nebulizer gas flow in a manner similar to dissolved ions We conclude that particle generated interferences must be avoided or eliminated to ensure accurate nanometrology.

1. Introduction:

The emergence of nanotechnology and associated fields has resulted in a need for analytical techniques to quantify nanoparticles (NPs) in both environmental and laboratory samples. Among them, single particle inductively coupled plasma mass spectrometry (spICP-MS) has emerged as the preferred technique to provide high throughput inorganic NP characterization. By acquiring an ICP-MS signal at a high time resolution, individual NPs that are ablated and ionized in the plasma produce discrete ion clouds that generate peaks in time-resolved data, with peak areas corresponding to the mass of a given element in an NP. spICP-MS can analyze thousands of NPs in aqueous suspension per minute, and can provide size detection limits below 10nm, dependent on the element sensitivity.[1] It is therefore the preferred technique to analyze NPs at environmentally relevant and/or ultra-trace concentrations, and is employed in various fields ranging from medicine to geochemistry.[2–4] Although the technique is well established, further progress can be made to improve its capability to accurately measure NPs.

A ubiquitous problem in quadrupole based ICP-MS analysis is the presence of spectral interferences, including isobaric, doubly charged, and polyatomic interferences. Methods for eliminating spectral interferences have been established, including correction equations or the use of multiple quadrupoles

with a collision/reaction cell.[5] Mathematical equations involving multiple isotopes of the interferent are most often used to correct for isobaric interferences, and in some cases, empirical equations can be used to correct for polyatomic interferences, such as rare earth element (REE) oxides.[6] However, for most polyatomic interferences, a cell gas is used in either collision or reaction mode to physically or chemically alter the analyte or interferent in order to accurately measure the analyte.[7] While all of these methods have been well established for ICP-MS analysis of dissolved analytes, the complete elimination of spectral interferences in spICP-MS has not been achieved. Studies of spectral interferences in spICP-MS analysis focus primarily on the elevated background signal generated from isobaric or polyatomic interferences. For example, the effect of interferences caused by matrix components and plasma gas on analysis of Fe, Zn, and Cr NPs was recently studied.[8]

In contrast, particle generated polyatomic and doubly charged interferences in spICP-MS have received little attention, and the few studies considering them do not provide a comprehensive investigation.[9] We hypothesize that during ablation and ionization in the plasma, NPs behave similarly to dissolved ions, and therefore a fraction of the ion cloud from an individual NP will be converted to polyatomic ions or doubly charged ions. If the ion cloud is large enough, the fraction of ions that form polyatomic or doubly charged species will be recorded as a peak in the mass spectrum, resulting in false positive particle detections for certain elements. We present two cases where these interferences are likely to be problematic due to elements with relatively high environmental abundance (Y and Nd) interfering on elements with low abundance (Ge, As, and Pd). Particle generated interferences are likely not limited to these analyte/interferent combinations, others may include Ga and Se, resulting from doubly charged lanthanides. Strategies to eliminate particle generated interferences are presented and discussed.

2. Methods and Materials:

A PerkinElmer NexION 350D ICP-MS was equipped with a glass cyclonic spray chamber, a concentric nebulizer, and nickel cones for both dissolved and single particle (sp) analysis. For sp analysis, transport efficiency (TE) was calculated using the particle size method with citrate-stabilized 50nm Au spheres (NanoComposix, San Diego, CA).[10] For sp mode, the dwell time was 100µs,the flow rate was 330µL min^{-1}, and data acquisition time was 60s. Instrument sensitivity was determined for each element using 10µg L^{-1} dissolved standards prepared by diluting 10mg L^{-1} stock solutions (Inorganic Ventures, Christiansburg, VA) in 2% nitric acid (trace metal grade, Fisher Scientific, Waltham, MA). The same standards were analyzed in solution mode to determine interference ratios, where data was integrated over 500ms. No internal standards were used to ensure the same conditions existed in both solution analysis and spICP-MS analysis.

Nano powders of Nd (Nd_2O_3), Y (Y_2O_3), and Pd (>99.9% purity) were purchased from Sky Spring nanomaterials (Houston, TX). Although particle sizes of 20-50nm were reported by the manufacturer, spICP-MS analysis showed polydisperse size distributions, likely due to a high degree of aggregation. A small (mg) quantity of each nano powder was suspended in a 0.1% w/w solution of sodium dodecyl sulfate (SDS, Fisher Scientific, Waltham, MA) and sonicated for 30 minutes to disaggregate particles. The suspensions were filtered through 0.45µm nylon syringe filters (Agilent, Santa Clara, CA) both to protect the nebulizer from large aggregates, and to remove large particles that would suffer from incomplete ablation in the plasma. The filtered suspensions were diluted 100x – 100,000x in 0.1% SDS and sonicated for an additional 5 minutes prior to spICP-MS analysis. For analysis of Nd-NPs, ^{144}Nd, ^{146}Nd, ^{150}Nd, ^{155}Gd, ^{160}Gd, ^{70}Ge, ^{72}Ge, ^{73}Ge and ^{75}As were monitored. For analysis of Y-NPs, ^{89}Y, ^{105}Pd, and ^{106}Pd were

monitored. ^{105}Pd was monitored in standard mode (no cell gas) and using the dynamic reaction cell (DRC) with an NH_3 flow rate of 1.0 mL min^{-1}. The Syngistix software (PerkinElmer, v2.5) was used to collect and process data. Additional data processing was performed in MATLAB (Mathworks, v2023). Particle detection thresholds (number of counts above which signals are recorded as particle events) were determined through an iterative process described elsewhere, and thresholds below 2 counts were manually adjusted to 2 counts to avoid false positives.[11] Particles were sized by converting peak areas to mass using the mass flux calibration curve (Equations S1, S2), then converting to an equivalent spherical diameter by assuming an oxide composition (Y_2O_3 and Nd_2O_3), or pure elemental composition (Pd, Ge, As), and a spherical shape (Equation S3).[10] For particle generated interferences, peaks were sized as Pd, Ge, and As to compare the false positives to sizes reported for these particle types in the literature, and thus assess the significance of the interference.

The magnitude of each interference (referred to as the "interference ratio") was measured in solution mode by analyzing dissolved standards of Y and Nd (10µg L^{-1}) and monitoring all isotopes listed above. The counts per second (cps) measured for the analytes (Ge, As, Pd) were divided by the cps measured for the interferents (Y, Nd), both signals were blank-subtracted. The same process was applied to spICP-MS data to calculate the interference ratios in sp mode; the signal recorded over the 60s analysis was summed for each analyte and interferent.

3. Results and discussion:

3.1: Particle generated oxide interferences, and elimination with cell technology

A suspension of Y-NPs was analyzed by spICP-MS to investigate the presence of particle generated oxide interferences that cause false NP detections. Y was chosen for several reasons. First, the rare earth elements (REEs) including Y readily form oxides in the ICP.[6] Second, the YO^+ ion has an m/z of 105, interfering on the only isotope of Pd without isobaric interferences.[12] The problem is significant in this case because Y is nearly three orders of magnitude more abundant in the upper continental crust than Pd, and is monoisotopic.[13] Figure 1 presents particle size distributions (PSDs) for the 3 isotopes monitored for the Y-NP analysis; ^{89}Y (a), ^{106}Pd (b), and ^{105}Pd (c). ^{105}Pd is also presented in (d) with the use of pure NH_3 as a reaction gas in the DRC.

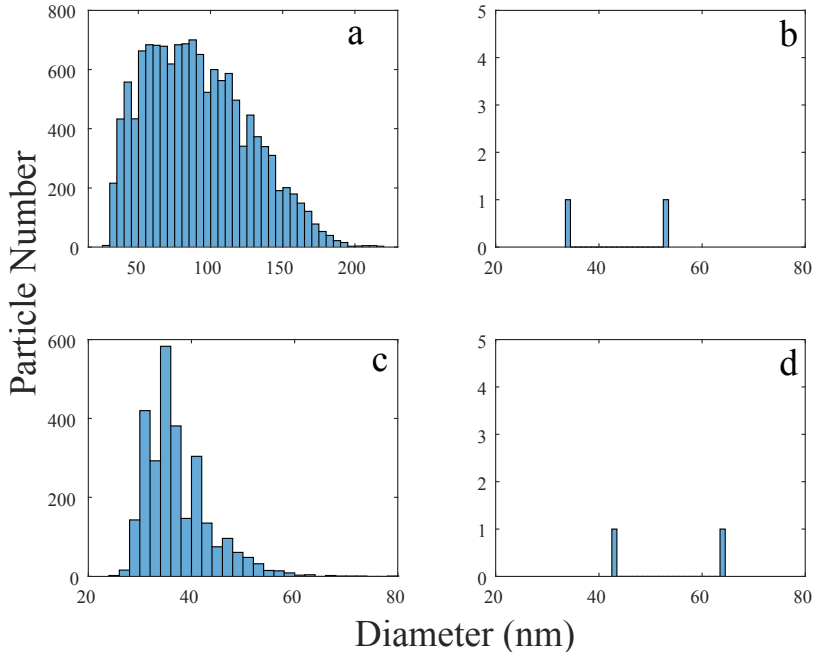

Figure 1: Particle size distributions resulting from spICP-MS analysis of a yttrium oxide nanoparticle suspension, including PSDs for ^{89}Y (sized as Y_2O_3) (a), ^{106}Pd (b), and ^{105}Pd (c), all analyzed without cell gas. ^{105}Pd was also analyzed with pure NH_3 in the dynamic reaction cell (d). Note that only Y-NPs were analyzed; the particles in (c) are $^{89}Y^{16}O$ peaks, generating false positives on ^{105}Pd.

The PSDs presented in Figure 1 clearly demonstrate the significance of particle generated oxide interferences. The PSD for ^{89}Y had a broad size distribution ranging from 30-200nm, likely resulting from a high degree of aggregation (Figure 1a). This is typical of suspended nano powders, even with extended sonication. Relevant parameters of the Y-NP suspension are detailed in Table S1. Figure 1b (^{106}Pd) shows just 2 peaks identified as particles indicating that no Pd was present in the NP suspension. Peaks on ^{106}Pd could be generated by $^{89}Y^{17}O$ or $^{89}Y^{16}OH$, however because only 2 peaks were detected, there is not a significant interference issue on ^{106}Pd due to Y. This is consistent with the low abundance of ^{17}O and ^{16}OH in the plasma.[14] In contrast, 2500 particles were detected for ^{105}Pd when no cell gas was used, indicating the presence of peaks generated by $^{89}Y^{16}O^+$ ion clouds (Table S1). The ^{105}Pd peaks are significantly lower in intensity than the ^{89}Y peaks, corresponding to the minor fraction of oxide species generated, in this case 1.12% (Table S2). When sized as Pd particles (Equation S3), the peaks generated from YO^+ ion clouds ranged from 25-80nm. Studies concerning the behavior of Pd NPs in environmental samples often report Pd NPs in this size range, indicating that any Y NPs in such samples would likely generate false positive Pd NPs.[15] Y NPs are likely to occurr at significant concentrations in many environmental samples, as the upper continental crust contains 21 mg Y Kg^{-1}.[13] The suspension of Y-NPs was analyzed using NH_3 in the DRC of the instrument to chemically eliminate the YO^+ interference. ^{105}Pd was monitored, and only 2 peaks were identified as particles, indicating that the DRC was successful in eliminating the interference (Figure 1d). Time resolved data for all isotopes monitored is presented in Figure S1.

To determine whether the YO^+ interference could be eliminated while still quantifying true Pd NPs, mixed suspensions of Y- and Pd-NPs were analyzed. The same concentration of Pd-NPs was used for all

samples, while the concentration of Y-NPs was varied by 500x (by performing varying dilutions of the stock suspension) to assess the ability to eliminate the interference over a broad range of interferent concentrations. Y and Pd particle numbers for each mixture are presented in Figure 2.

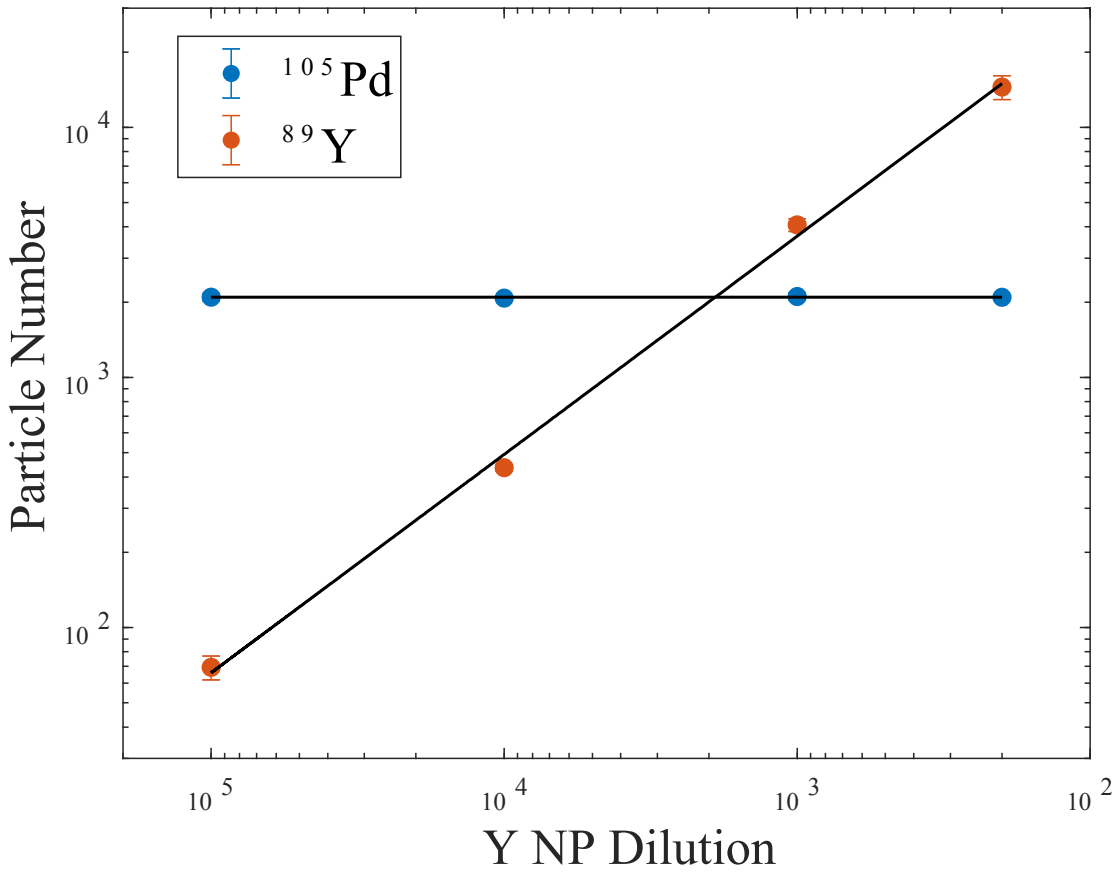

Figure 2: Number of particles detected in a 60s spICP-MS analysis of mixed Y- and Pd- nanoparticle suspensions. Y-NP dilution refers to the dilution factor of the stock suspension prepared from powder. The Pd stock suspension was diluted by 1000x for all 4 mixtures. Error bars represent one standard deviation of triplicate analysis (many are too small to be visible).

The trends in particle number presented in Figure 2 indicate that the increasing concentration of Y-NPs in the mixtures had no effect on the number of Pd NPs analyzed. As the Y-NP dilution factor decreased (from left to right), the detected number of Y-NPs increased from 70 ± 10 to 14,500 ± 1600 (Table S3). However, there was not a significant difference in the number of Pd-NPs detected in all four mixtures, which ranged from 2070 ± 30 to 2130 ± 50 (Table S3).

Although the YO^+ interference was successfully eliminated using the DRC, the ability to measure Pd-NPs is affected in two ways when compared to standard mode. Sensitivity was reduced by 27% in DRC mode (Figure S2) and the interaction between the ion clouds and the cell gas resulted in peak broadening, a well-documented phenomenon in spICP-MS analysis (Figure S3).[16] These two effects resulted in a higher

particle detection threshold caused by "non-resolved" particles, commonly observed in polydisperse samples (to resolve these particles, additional dilutions would be needed).[17] The reduced sensitivity and elevated threshold led to under-counting of particles when using DRC mode for a neat suspension of Pd-NPs (Table S1). The mean size of Pd-NPs also differed between the two modes of operation; in DRC mode, the average diameter was 97 nm, compared to 82nm without a reaction gas (Table S1). This difference arises from the elevated particle detection threshold; the smallest particles are not detected in DRC mode, and thus the average diameter is larger and particle number is lower. Particles are still sized accurately in both modes of operation (instrument sensitivity was calibrated in both modes, Figure S2), but average diameter is a poor indicator of the PSD in this case. The elimination of the YO^+ interference and resulting false positive Pd-NPs is more important for environmental applications than underreporting true Pd-NP numbers and increasing mean size, and therefore DRC mode is preferred.

3.2: Particle generated doubly charged interferences

To assess the effects of particle generated doubly charged interferences in spICP-MS analysis, a suspension of Nd-NPs was analyzed and several key isotopes were monitored. Nd was chosen because of its relatively low second ionization potential (resulting in Nd^{2+}) and because of its abundance in environmental matrices. Because Nd has 7 naturally occurring isotopes, many interferences are generated from Nd-NPs. Figure 3 presents PSDs for Nd and resulting interferences on As and Ge.

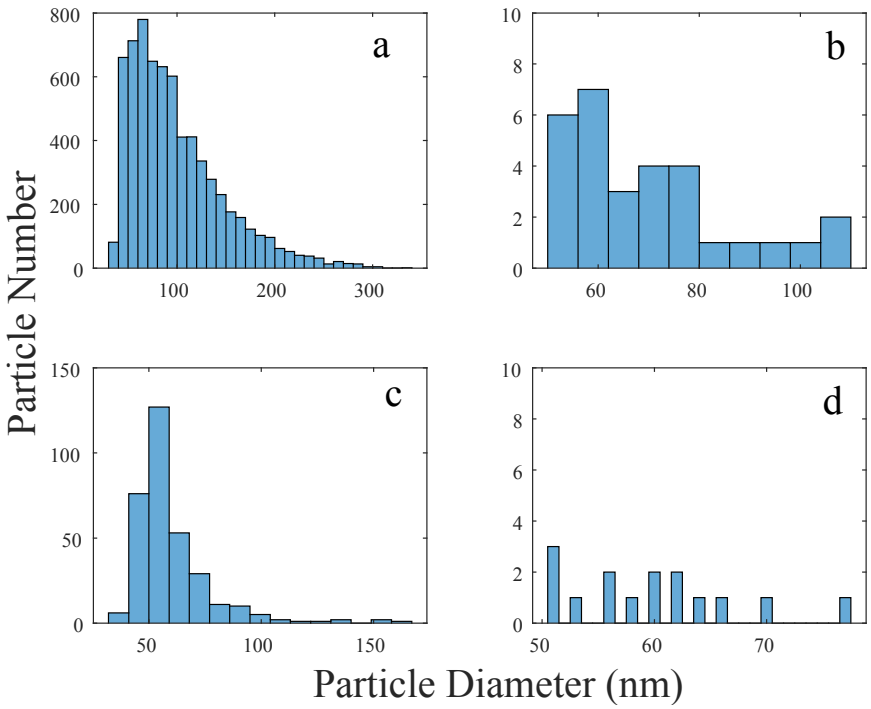

Figure 3: Particle size distributions resulting from spICP-MS analysis of a neodymium oxide nanoparticle suspension, including PSDs for ^{144}Nd (Sized as Nd_2O_3) (a), ^{75}As (b), ^{72}Ge (c), and ^{70}Ge (d).

The PSDs in Figure 3 indicate that Nd NPs generated false positive particles for ^{72}Ge and ^{75}As due to the doubly charged interference. Similar to the Y PSD in Figure 1a, the Nd PSD (Figure 3a) is polydisperse, ranging from 40-300nm. The PSD for ^{75}As is presented in Figure 3b, where 30 false positive particles

were detected ranging from 50-110nm (when sized as pure As NPs), generated from $^{150}Nd^{2+}$ (Table S1). Only 1 particle was detected in a blank sample (Table S4). False positive peaks occurring on ^{75}As presents a significant issue because As is monoisotopic, and therefore a clean isotope cannot be chosen. Additionally, detection of ultra-trace As in environmental samples is important due to its toxicity, as well as its application in mineral exploration as a pathfinder element.[18,19] Figure 3c and 3d present PSDs for ^{72}Ge and ^{70}Ge, respectively. The Nd^{2+} interference generated 900 false positive particles for ^{72}Ge (Table S1); the higher number compared with ^{75}As arising from the isotopic distribution of Nd. ^{144}Nd accounts for 23.8%, while ^{150}Nd accounts for just 5.6%. 15 particles were detected for ^{70}Ge, which could have arisen from several sources including Ce contamination in the Nd-NPs (creating Ce^{2+} peaks), or due to an isobaric interference with Zn, a common contaminant in ICP-MS analysis. Eliminating false Ge particles may not be as critical as Pd or As in environmental samples, but Ge NPs are used in advanced technologies including solar cells and batteries, making the identification of false positives important.[20,21]

spICP-MS analysis of the Nd-NP suspension clearly indicates that the fraction of ion clouds that are doubly charged can generate false positive particles. However, unlike for YO^+, NH_3 could not be used to eliminate these interferences. As an alternative, mass shifting is often used by reacting O_2 with the ions (i.e. to create AsO, monitoring m/z 91).[22] A high resolution ICP-MS such as a sector field (SF-ICP-MS) can also provide the resolution needed to resolved doubly charged interferences, or multiple quadrupoles can be used to eliminate the interferant.[9,23] On a quadrupole ICP-MS, extreme care must be taken to avoid particle generated doubly charged interferences. Screening environmental samples for suspected interferants based on isotopic distributions, crustal abundances, and second ionization potentials is suggested as the best means to avoid reporting spICP-MS data with false positives.

3.3: Variation in nebulizer gas flow rate influences interference formation

To provide additional evidence for the mechanism of formation of particle generated interferences, nebulizer gas flow rate was varied during spICP-MS analysis of Nd-NPs, monitoring ^{72}Ge, ^{160}Gd, and ^{144}Nd. The fraction of ions for each interference ($^{144}Nd^{16}O^+$ as ^{160}Gd, and Nd^{++} as ^{72}Ge) was plotted for each nebulizer flow rate tested, shown in Figure 4.

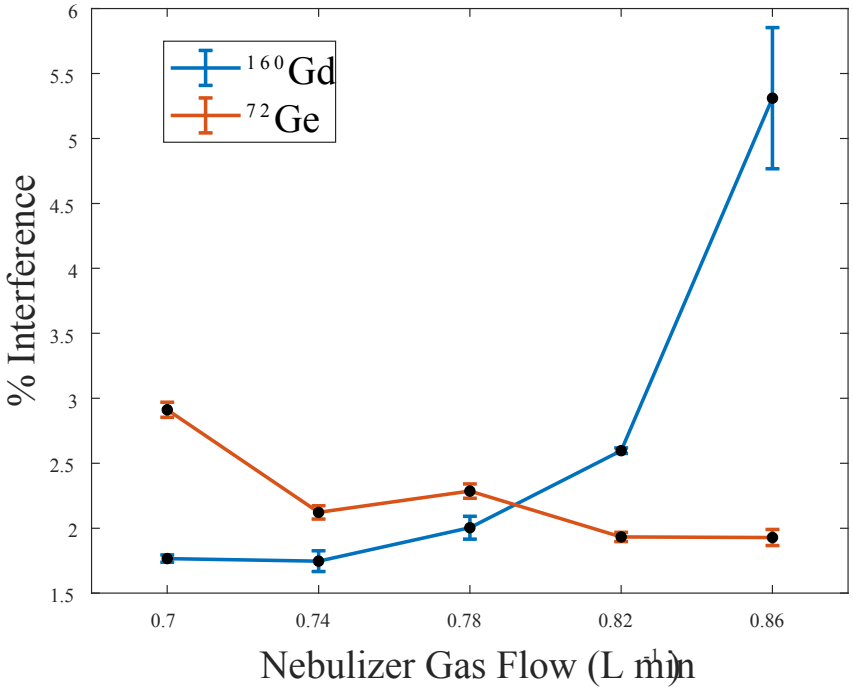

Figure 4: Magnitude of Nd^{2+} (^{72}Ge) and $^{144}Nd^{16}O^{+}$ (^{160}Gd) interferences recorded in single particle mode as a function of nebulizer gas flow rate. The % interference was calculated by dividing the summed counts measured on ^{72}Ge and ^{160}Gd by the counts measured on ^{144}Nd, and multiplying by 100%. Error bars represent one standard deviation of triplicates.

Figure 4 demonstrates that for spICP-MS analysis, nebulizer gas flow rate significantly affects the formation of oxide and doubly charged interferences. Increasing the nebulizer gas flow rate results in several changes to sample introduction. The transport efficiency is increased, and as a result the sensitivity of dissolved ions increases. However, an increase in nebulizer flow rate also results in a shorter duration of the molecules/ions in the plasma, which leads to increased oxide formation, and decreased double charge formation.[24,25] This is reflected in an increased signal observed for all isotopes monitored, as a result of increased transport into the plasma with increasing nebulizer flow rate (Table S5). Interference formation was also affected, with an increase in the fraction of oxides (^{160}Gd increases from 1.8 to 5.3%) and a decrease in the fraction of doubly charged ions (^{72}Ge decreases from 2.9 to 1.9%) measured as nebulizer gas flow rate increased from 0.7 to 0.86L min^{-1}. This suggests that the mechanism of interference formation from spICP-MS analysis of NP suspensions is similar to that of dissolved ions, the latter being extensively reported in the literature.[5] 3.4: Comparing spectral interferences between spICP-MS and solution ICP-MS:

Interference ratios were calculated for both sp mode and solution mode for all combinations of analyte and interferent discussed above. The ratios are plotted in Figure5 and recorded in Table S2.

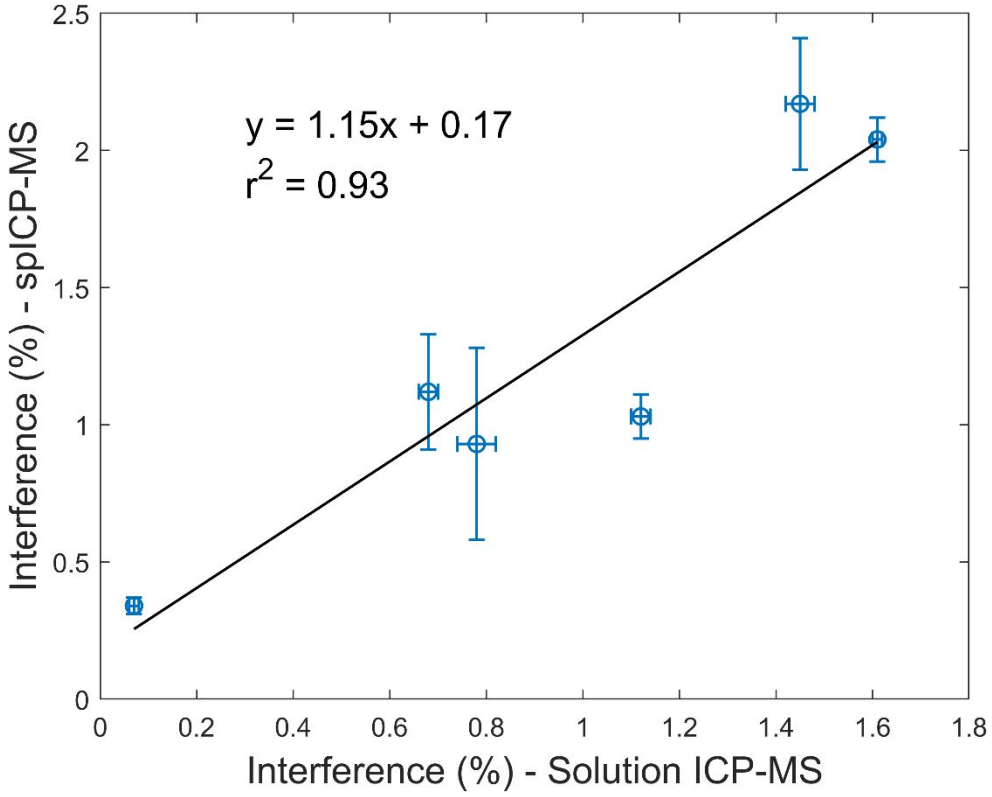

Figure 5: YO^+, NdO^+, and Nd^{2+} interferences determined from solution ICP-MS analysis of dissolved Y and Nd standards, and from spICP-MS analysis of Y and Nd nanoparticle suspensions. Interferences were calculated by dividing the counts recorded on the analyte (Pd, As, Ge, Gd) by the counts recorded on the major isotope generating the interference (Y, Nd) and multiplying by 100%. Error bars represent one standard deviation of triplicate analysis.

The interference ratios for spICP-MS and solution ICP-MS are highly correlated ($r^2 = 0.93$) and have a slope close to unity (m = 1.15), indicating that similar processes in the ICP generate interferences in both modes of analysis. However, unlike solution mode, where a correction can be applied to subtract the counts contributed by the interferent, single particle data cannot be corrected in this manner. This is because spICP-MS analysis using a quadrupole mass analyzer can only detect one element at a time. In an environmental sample containing particles with multiple elements, for example Y and Pd, the data would be reported as separate PSDs for Y and Pd. There is no way to subtract off the YO^+ interference from individual Pd-NPs, because of the polydispersity of Y-NPs in an environmental sample coupled with the inability to measure multiple elements simultaneously. Thus the differing contributions of YO^+ to each Pd particle cannot be determined. Uncertainty in the interference ratio was greater for sp mode, likely because NP suspensions are not homogeneous as dissolved solutions are, especially for the highly polydisperse suspensions considered in this study. Relatively few Nd- and Y-NPs were detected at large sizes (>200nm); these are likely to generate the highest number of counts for polyatomic and doubly charged species. Poor representativity of these large particles leads to greater uncertainty in the interference ratio. Although the slope is close to 1, we hypothesize that it is slightly higher than 1 (1.15) due to issues with detecting high count rates associated with large particles. Because the dual detector could not be used in sp mode (with the Syngistix V2.5 software), particles generating over $2x10^6$ cps (1600 counts in a 100µs dwell time) are not recorded in the raw data. However, the particles large

enough to generate this number of counts are likely still completely ablated, meaning the doubly charged or oxide fraction of the ion cloud is still detected, resulting in a slope >1. A recent release of the Syngistix software enables use of the dual detector, possibly negating this effect.

4. Conclusions:

From this study we conclude that particle generated spectral interferences are likely to occur in spICP-MS analysis, and have the potential to significantly impact results for environmental or laboratory samples. Analysis of Y- and Nd-NPs, both of which are abundant in environmental matrices, resulted in significant numbers of false positive particles for trace elements Pd, As, and Ge due to fractions of the ion clouds forming doubly charged or oxide species. For spICP-MS analysis of environmental samples, extreme care must be taken to avoid these interferences. We recommend screening samples for environmentally abundant elements that have a high propensity to form polyatomic or doubly charged species.[12] The Dynamic Reaction Cell (DRC) can then be used to chemically or physically eliminate many of these interferences, or more advanced instrumentation may be required. Higher sensitivity provided by a magnetic sector instrument could negate interference issues by resolving the difference in mass between the analyte and interferent. Additionally, the multi-elemental capability of spICP-Time-of-Flight-MS could be used to correct single particle data for interferences, if the magnitude of the interference was tested. Further work is needed to establish best practices to avoid particle generated interferences on a variety of instrument types.

Acknowledgements:

This work was supported by the United States Army Corps of Engineers (Grant No. W912HZ-21-2-0049).

Department of Chemistry. **References:**

1 S. Lee, X. Bi, R. B. Reed, J. F. Ranville, P. Herckes and P. Westerhoff, *Environ. Sci. Technol.*, 2014, **48**, 10291–10300.

2 M. D. Montaño, J. W. Olesik, A. G. Barber, K. Challis and J. F. Ranville, *Anal. Bioanal. Chem.*, 2016, **408**, 5053–5074.

3 M. F. Hochella, D. W. Mogk, J. Ranville, I. C. Allen, G. W. Luther, L. C. Marr, B. P. McGrail, M. Murayama, N. P. Qafoku, K. M. Rosso, N. Sahai, P. A. Schroeder, P. Vikesland, P. Westerhoff and Y. Yang, *Science (80-.).*, 2019, 363.

4 A. J. Goodman and J. F. Ranville, *J. Geochemical Explor.*, 2023, **251**, 107231.

5 T. Lum and K. S. Leung, *J. Anal. At. Spectrom.*, 2016, **31**, 1078–1088.

6 M. G. Lawrence, A. Greig, K. D. Collerson and B. S. Kamber, *Appl. Geochemistry*, 2006, **21**, 839–848.

7 M. Colon, M. Hidalgo and M. Iglesias, *J. Anal. At. Spectrom.*, 2009, **24**, 518–521.

8 I. Kálomista, A. Kéri and G. Galbács, *J. Anal. At. Spectrom.*, 2016, **31**, 1112–1122.

9 K. Chun, J. T. Lum and K. S. Leung, *Anal. Chim. Acta*, 2022, **1226**, 340258.

10 H. E. Pace, N. J. Rogers, C. Jarolimek, V. A. Coleman, C. P. Higgins and J. F. Ranville, *Anal. Chem.*,

2011, **83**, 9361–9369.

11 F. Laborda, A. C. Gimenez-Ingalaturre, E. Bolea and J. R. Castillo, *Spectrochim. Acta - Part B At. Spectrosc.*, 2020, **169**, 105883.

12 T. W. May and R. H. Wiedmeyer, *At. Spectrosc.*, 1998, **19**, 150–155.

13 R. L. Rudnick, *The Crust*, 2005.

14 L. A. Currie, *Anal. Chem.*, 1968, **40**, 586–593.

15 K. Ki, J. Jiménez-lamana, J. Kowalska, B. Krasnod and J. Szpunar, 2018, **615**, 1078–1085.

16 E. Bolea-fernandez, D. Leite, A. Rua-ibarz, T. Liu, G. Woods, M. Aramendia, M. Resano and F. Vanhaecke, *Anal. Chim. Acta*, 2019, **1077**, 95–106.

17 S. Beavers, C. Smith, S. Brown, N. Malone, D. H. Fairbrother, A. Goodman and J. F. Ranville, *Environ. Sci. Nano*, , DOI:10.1039/D3EN00425B.

18 L. W. Ashton and W. C. Riese, *J. Geochemical Explor.*, 1989, **31**, 171–184.

19 M. F. Hughes, *Toxicol. Lett.*, 2002, **133**, 1–16.

20 C. Zhang, Z. Li, X. Deng, B. Yan, Z. Wang and X. Chen, *Sol. Energy*, 2019, **188**, 839–848.

21 R. Mo, Z. Lei, D. Rooney and K. Sun, *ACS Nano*, 2019, **13**, 7536–7544.

22 F. C. Pinheiro, C. D. B. Amaral, D. Schiavo and J. A. Nóbrega, *Food Anal. Methods*, 2017, **10**, 992–998.

23 M. Hadioui, G. Knapp, A. Azimzada, I. Jreije, L. Frechette-Viens and K. J. Wilkinson, *Anal. Chem.*, 2019, **91**, 13275–13284.

24 V. Balaram, , DOI:10.1002/rcm.9065.

25 B. Hattendorf, B. Gusmini, L. Dorta and R. S. Houk, , DOI:10.1021/acs.analchem.6b01614.